Effect of losses on the visibility of mesoscopic entanglement

Giacomo M. D'Ariano, Matteo G. A. Paris, and Massimiliano F. Sacchi
Theoretical Quantum Optics Group, INFM Unità di Pavia, Dipartimento di Fisica ''Alessandro Volta,'' Università di Pavia, Via Bassi 6, I-27100 Pavia, Italy

Francesco De Martini
Dipartimento di Fisica and Istituto Nazionale per la Fisica della Materia, Università di Roma ''La Sapienza,'' Roma 00185, Italy
(Received 10 June 1999; published 16 May 2000)

The effect of losses on the visibility of mesoscopic entanglement states is analyzed on the basis of a recently proposed generation scheme which amplifies a *quantum seed* through stimulated down-conversion. The visibility of the entanglement is shown with the amplifier working above threshold, for short interaction times.

PACS number(s): 42.50.Dv, 03.65.Bz

I. INTRODUCTION

The recent developments in quantum optics and light manipulation of atoms and ions have renewed interest in the basic laws of quantum mechanics, with the main focus on the superposition principle and the existence of nonlocal correlations among separate systems, the so-called ''entanglement.'' The superposition principle and the entanglement—the two inherent quantum features that are the basis of the quantum information technology [1]—have been extensively studied both theoretically and experimentally [2], leading to the new concept of ''quantum teleportation'' that has been recently demonstrated in several experiments [3]. These research lines motivated the search for methods of preparation and measurement of quantum states [4]. While quantum tomography [5] certainly represents a solution to the measurement problem, the state-preparation issue is still under way. For entangled ''twin beams'' of radiation, parametric down-conversion represents the ideal state-preparation tool [6], and these states have been used in a series of quantum mechanical tests, including Bell's inequalities [7] and secure key distribution [8]. However, both problems of generation and measurement become very difficult when the superposition/entanglement involves ''mesoscopic'' states—the issue of the Schrödinger-cat states—because such superpositions are very fragile to any kind of noise. In Ref. [9] a scheme has been proposed for generating mesoscopic entangled superpositions, based on quantum injection into a non-degenerate parametric amplifier operating in an entangled configuration. This scheme has been analyzed in the case of parametric oscillations, with nonlinear crystals placed in optical cavities [10]. The scheme has been improved in Refs. [11,12], where the dynamics of the amplifier is restricted to two modes only—the signal and the idler—that share the entanglement on their wave vectors, with the *seed* photon injected in a way that makes signal and idler paths indistinguishable. Since this improved scheme is very promising, in principle, for the generation of mesoscopic entanglement, the crucial effect of noise in the measurement stage needs to be analyzed. Here, in this paper, we study the effect of losses on the visibility of such mesoscopic entanglement, and show that a realistic amplification process preserves the path indistinguishability while enhancing to mesoscopic scale the number of photons at the output. This leads to the generation of a mesoscopic superposition that is quite robust against decoherence.

In Sec. II we briefly review the generation scheme in the absence of losses. There, we also suggest a feasible measurement to reveal the output mesoscopic superposition. The realistic amplification process is analyzed in Sec. III, taking into account the effects of losses. The whole state generation is numerically studied by means of Monte Carlo simulations. The appearance of mesoscopically entangled superpositions at the output, and their robustness against decoherence are demonstrated. Section IV closes the paper with some concluding remarks.

II. THE IDEAL DYNAMICS

In this section we briefly review the scheme of Refs. [11,12] for generating mesoscopic entanglement through stimulated down-conversion of a quantum seed. The seed is obtained as a result of state reduction on a down-converted pair of photons by a triggering photodetector. In addition, an effective measurement scheme is suggested to reveal the mesoscopic quantum superposition at the output.

A. Generation of the seed state

A nondegenerate optical parametric amplifier (NOPA) consists of a $\chi^{(2)}$ nonlinear optical crystal cut for type-I phase matching. The crystal couples two modes with the same polarization according to the effective Hamiltonian

$$\hat{H}_\kappa = i\kappa(a^\dagger b^\dagger - ab), \tag{1}$$

where κ represents the effective nonlinear coupling, and a and b denote modes with wave vectors satisfying the phase-matching condition $\vec{k}_a + \vec{k}_b = \vec{k}_p$, $\vec{k}_p$ being the wave vector of the pump. For weak pumping and short interaction time τ, the state exiting the NOPA by spontaneous down-conversion (SPDC) is approximated by

$$|\Psi\rangle = \frac{1}{\sqrt{1+(\kappa\tau)^2}}[|\mathbf{0}\rangle + \kappa\tau|1\rangle_a|1\rangle_b], \tag{2}$$

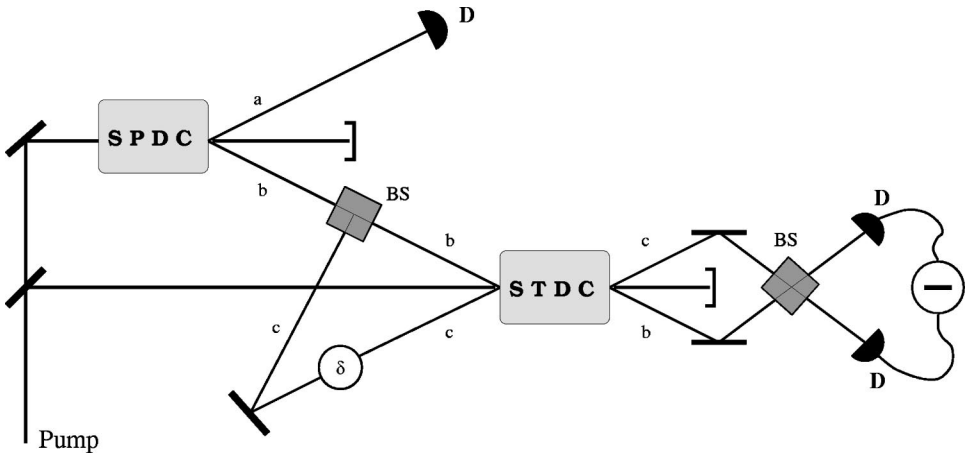

FIG. 1. Schematic diagram of the setup for the generation of mesoscopically entangled quantum superpositions by parametric amplification of a single photon state prepared in a way that makes signal and idler paths indistinguishable. In the first part a single-photon state is prepared by a conditional measurement on a spontaneously down-converted (SPDC) beam. The input state for the second crystal is thus given by $|\Phi\rangle=(1/\sqrt{2})\{|1\rangle_b|0\rangle_c+e^{i\delta}|0\rangle_b|1\rangle_c\}$. This quantum injection triggers a stimulated down-conversion process (STDC) which leads to the desired mesoscopic quantum superposition. Both spontaneous and stimulated down-conversion take place in nondegenerate optical amplifiers (NOPA) consisting of nonlinear $\chi^{(2)}$ crystals cut for type-I phase matching. In the last stage of the setup the output beams from the second crystal are mixed in a beam splitter (BS) and then detected. The mean value of the difference photocurrent gives the second-order correlation function $\mathsf{C}^{(2)}$ defined in Eq. (11) of the text.

where $|\mathbf{0}\rangle$ denotes the vacuum state and $|n\rangle_i$ the state with n photons in the ith mode. Let us now consider the conditional measurement scheme depicted in the left part of Fig. 1. One of the down-converted beams is probed by the photodetector D, and after reduction (on successful photodetection), the mode b enters a 50/50 beam splitter (BS), so that the resulting state can be written as (see Fig. 1)

$$|\Phi\rangle=\frac{1}{\sqrt{2}}\{|1\rangle_b|0\rangle_c+e^{i\delta}|0\rangle_b|1\rangle_c\}, \tag{3}$$

where δ is a tunable phase shift which results from the difference in the optical paths of modes b and c. Notice that the BS scatters the impinging photon into two directions with equal probability amplitude, thus making the two possible paths of the photon indistinguishable. As shown in the following, such path indistinguishability plays the role of a *quantum seed*, which makes the parametric amplification of the state (3) a source of mesoscopically entangled quantum superpositions.

B. From path indistinguishability to mesoscopic entanglement

In the following we analyze the parametric amplification which takes place in the second crystal of the scheme in Fig. 1. For this crystal the input signal is not the e.m. vacuum, but the single-photon state of Eq. (3). Therefore, we are dealing with a kind of *stimulated* down-conversion process. After the beam splitter, the two modes of Eq. (3) can be directed to the second crystal with the proper wave vectors in order to satisfy phase-matching conditions. In such a way, the relevant dynamics in the second crystal involves modes b and c, according to the NOPA interaction Hamiltonian $\hat{H}_\kappa=i\kappa(b^\dagger c^\dagger-bc)$

The use of the balanced beam splitter before the second crystal is a relevant point of the method. On one hand, it allows us to restrict the relevant NOPA dynamics to two modes only; on the other hand, it is the key ingredient to make the two paths for the photon indistinguishable, thus leading to the initial quantum seed described in Eq. (3). Notice that in the schemes of Refs. [9,10] four modes are involved in the amplification stage. The presence of many modes makes the effect of losses more detrimental, thus leading to a more stringent decoherence. For this reason, the schemes of Refs. [11,12] and the present one should be more effective in generating mesoscopic quantum superpositions.

The amplifier described by Hamiltonian $\hat{H}_\kappa$ is characterized by the gain $\mathcal{G}$, which is given by $\mathcal{G}=\cosh^2(\kappa\tau)$, τ being the interaction time. In the case of ideal amplification (no losses), the state at the output writes

$$|\Phi_{OUT}\rangle=\frac{1}{\sqrt{2\mathcal{G}}}\sum_{n=0}^{\infty}\left(\frac{\mathcal{G}-1}{\mathcal{G}}\right)^{n/2}\sqrt{1+n}\{|n+1\rangle_b|n\rangle_c+e^{i\delta}|n\rangle_b|n+1\rangle_c\}. \tag{4}$$

The state in Eq. (4) describes two highly correlated and spatially separated beams. For large enough gain it represents a kind of mesoscopically entangled quantum superposition, whose mean photon number is given by

$$\langle\Phi_{OUT}|b^\dagger b+c^\dagger c|\Phi_{OUT}\rangle=4\mathcal{G}-3. \tag{5}$$

We now evaluate the two-mode Wigner function, which is defined as follows:

$$W(x_1,y_1;x_2,y_2)$$
$$= \int d\mu_1 \int d\nu_1 \int d\mu_2 \int d\nu_2 e^{2i(\nu_1 x_1 - \mu_1 y_1 + \nu_2 x_2 - \mu_2 y_2)}$$
$$\times \mathrm{Tr}\{\hat{\varrho}\hat{D}_c(\mu_1 + i\nu_1)\hat{D}_b(\mu_2 + i\nu_2)\}. \quad (6)$$

In Eq. (6) the variables (x_1,y_1) and (x_2,y_2) pertain to modes c and b, respectively, and $\hat{D}_a(z) = \exp[za^\dagger - \overline{z}a]$ denotes the displacement operator for mode a. For $\hat{\varrho} = |\Phi_{OUT}\rangle\langle\Phi_{OUT}|$ one obtains

$$W_\tau(x_1,y_1;x_2,y_2)$$
$$= \frac{8}{\pi^2}\exp[-(4\mathcal{G}-2)(x_1^2+x_2^2+y_1^2+y_2^2) - 8\sqrt{\mathcal{G}(\mathcal{G}-1)}$$
$$\times (X_1 x_2 + Y_1 y_2)][e^{-2\kappa\tau}(X_1 - x_2)^2$$
$$+ e^{-2\kappa\tau}(Y_1 - y_2)^2 - \tfrac{1}{2}], \quad (7)$$

where

$$X_1 = x_1 \cos\delta + y_1 \sin\delta,$$
$$Y_1 = -x_1 \sin\delta + y_1 \cos\delta. \quad (8)$$

As can be easily checked, the Wigner function in Eq. (7) shows negative values in a sizable region of the phase space, thus revealing the genuine nonclassical nature of the state resulting from stimulated down-conversion [9,12]. The high degree of entanglement of $|\Phi_{OUT}\rangle$ is revealed also by the two-mode photon number distribution, which, for any value of the phase shift δ, reads as follows:

$$P(n,m) = |{}_c\langle n|{}_b\langle m|\Phi_{OUT}\rangle|^2 = \frac{1}{2\mathcal{G}^2}\left(\frac{\mathcal{G}-1}{\mathcal{G}}\right)^{n-1}$$
$$\times \left[n\,\delta_{m,n-1} + (n+1)\frac{\mathcal{G}-1}{\mathcal{G}}\,\delta_{m,n+1}\right], \quad (9)$$

where δ_{kl} denotes the Kronecker delta. The two-mode number probability $P(n,m)$ is reported in Fig. 2 for two different values of the gain $\mathcal{G}$. The high degree of correlations in $P(n,m)$ is apparent. Notice that the location of the peaks linearly increases with the gain $\mathcal{G}$. It should be emphasized that the distributions in Fig. 2 are very different from the corresponding distribution of the so-called twin-beam state

$$|\Phi_{TWB}\rangle = \frac{1}{\sqrt{\mathcal{G}}}\sum_{n=0}^{\infty}\left(\frac{\mathcal{G}-1}{\mathcal{G}}\right)^{n/2}|n\rangle_b|n\rangle_c, \quad (10)$$

which results from spontaneous down-conversion. In the case of the twin beam state the number distribution $P(n,m)$ is just a two-mode thermal distribution $P(n,m) = \delta_{m,n}\mathcal{G}^{-1-n}(\mathcal{G}-1)^n$, and the quantum correlation involves only the photon number fluctuations, which are amplified by the down-conversion process. Actually, the Wigner function of the twin beam (i.e., the output state without the quantum injection) is positive over the whole phase space.

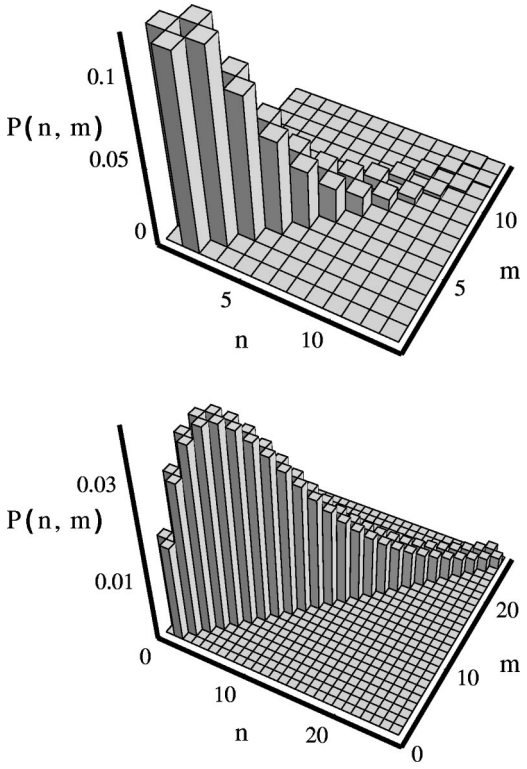

FIG. 2. The two-mode photon distribution $P(n,m)$ for two different values of the gain $\mathcal{G}$, $\mathcal{G}=2$ on the left and $\mathcal{G}=5$ on the right.

As a measurement scheme to check the generation of the mesoscopic superposition $|\Phi_{OUT}\rangle$, we suggest the detection of the second-order correlation function

$$\mathsf{C}^{(2)} = \mathrm{Tr}\{\hat{\varrho}(b^\dagger c + bc^\dagger)\}, \quad (11)$$

which can be accomplished by the following interference experiment. The output beams from the amplifier are mixed in a 50/50 balanced BS, and then the difference photocurrent is detected, as in a customary homodyne detection scheme (see Fig. 1). Using Eq. (4) it results

$$\mathsf{C}^{(2)} = \langle\Phi_{OUT}|b^\dagger c + bc^\dagger|\Phi_{OUT}\rangle = \frac{1}{2}(8\mathcal{G}-5)\cos\delta, \quad (12)$$

that is, one has interference fringes with amplitude and modulation that depend on the amplification gain and on the optical paths of the input beams, respectively. It is worth noticing that without quantum injection, i.e., for the twin-beam state, there is no interference effect, and one has

$$\mathsf{C}^{(2)} = \langle\Phi_{TWB}|b^\dagger c + bc^\dagger|\Phi_{TWB}\rangle = 0. \quad (13)$$

The effect of nonunit quantum efficiency of the photodetectors is simply a rescaling of the output photocurrent $\mathsf{C}_\eta^{(2)} = \eta\mathsf{C}^{(2)}$.

III. DYNAMICS OF THE STIMULATED DOWN-CONVERSION PROCESS

In the previous section we analyzed the stimulated down-conversion process in the ideal case of perfect amplification, namely without taking into account the effects of losses. Here, we consider a more realistic situation and study whether the state $|\Phi_{OUT}\rangle$ of Eq. (4) can be actually approached when losses unavoidably introduce decoherence effects. The realistic amplification process is described in terms of the two-mode Master equation

$$\frac{d\hat{\varrho}_t}{dt}\equiv\mathcal{L}\hat{\varrho}_t=-i[\hat{H}_\kappa,\hat{\varrho}_t]+\Gamma(L[c]\hat{\varrho}_t+L[b]\hat{\varrho}_t), \quad (14)$$

where $\hat{\varrho}_t\equiv\hat{\varrho}(t)$, $\hat{H}_\kappa$ is the NOPA interaction Hamiltonian, Γ denotes the damping rate, and $L[\hat{O}]$ is the Lindblad superoperator

$$L[\hat{O}]\hat{\varrho}_t=\hat{O}\hat{\varrho}_t\hat{O}^\dagger-\frac{1}{2}\hat{O}^\dagger\hat{O}\hat{\varrho}_t-\frac{1}{2}\hat{\varrho}_t\hat{O}^\dagger\hat{O},$$

which describes the effect of losses.

The Hamiltonian $\hat{H}_\kappa$ in the Master equation (14) strongly correlates the two modes. However, the unitary transformation

$$\hat{V}=\exp\left\{\frac{\pi}{4}(c^\dagger b-cb^\dagger)\right\} \quad (15)$$

''disentangles'' the Hamiltonian $\hat{H}_\kappa$ into two single-mode squeezing Hamiltonians, namely,

$$\hat{V}\hat{H}_\kappa\hat{V}^\dagger=\frac{i\kappa}{2}(c^{\dagger 2}-c^2)-\frac{i\kappa}{2}(b^{\dagger 2}-b^2). \quad (16)$$

At the same time, the sum of the Lindblad terms is left unchanged [13] by the transformation (15), namely,

$$\hat{V}\{L[c]+L[b]\}\hat{V}^\dagger=L\left[\frac{c-b}{\sqrt{2}}\right]+L\left[\frac{b+c}{\sqrt{2}}\right]$$
$$=L[c]+L[b]. \quad (17)$$

Therefore, the solution $\hat{\varrho}_t$ of Eq. (14) can be written as

$$\hat{\varrho}_t=\hat{V}^\dagger\hat{\varrho}'\hat{V}, \quad (18)$$

$\hat{\varrho}'_t$ being the solution of the ''disentangled'' Master equation

$$\frac{d\hat{\varrho}'_t}{dt}=(\mathcal{L}_c+\mathcal{L}_b)\hat{\varrho}'_t=\frac{\kappa}{2}[c^{\dagger 2}-c^2,\hat{\varrho}'_t]$$
$$+\Gamma L[c]\hat{\varrho}'_t-\frac{\kappa}{2}[b^{\dagger 2}-b^2,\hat{\varrho}'_t]+\Gamma L[b]\hat{\varrho}'_t. \quad (19)$$

The master equation (19) can be transformed into a Fokker-Planck equation for the two-mode Wigner function $W'_t(x_1,y_1;x_2,y_2)$. Using the differential representation of the superoperators in Eq. (19) the corresponding Fokker-Planck equation reads as follows:

$$\partial_\tau W'_\tau(x_1,y_1;x_2,y_2)$$
$$=[\tfrac{1}{8}(\partial^2_{x_1x_1}+\partial^2_{y_1y_1}+\partial^2_{x_2x_2}+\partial^2_{y_2y_2})+\gamma_+(\partial_{x_1}x_1+\partial_{y_2}y_2)$$
$$+\gamma_-(\partial_{x_2}x_2+\partial_{y_1}y_1)]W'_\tau(x_1,y_1;x_2,y_2), \quad (20)$$

where τ denotes the rescaled time $\tau=\Gamma t$, and the drift terms γ_+ and γ_- are given by

$$\gamma_\pm=\frac{1}{2}\left(1\pm\frac{2\kappa}{\Gamma}\right). \quad (21)$$

Notice the asymmetric drift terms in Eq. (20), which account for the squeezing terms in the Master equation (19).

The solution of Eq. (20) can be written as

$$W'_\tau(x_1,y_1;x_2,y_2)$$
$$=\int dx'_1\int dx'_2\int dy'_1\int dy'_2$$
$$\times W'_0(x'_1,y'_1;x'_2,y'_2)G_\tau(x_1|x'_1)G_\tau(x_2|x'_2)G_\tau(y_1|y'_1)$$
$$\times G_\tau(y_2|y'_2), \quad (22)$$

where $W'_0(x_1,y_1;x_2,y_2)$ is the Wigner function at $\tau=0$, and the Green functions $G_\tau(x_j|x'_j)$ are given by

$$G_\tau(x_j|x'_j)=\frac{1}{\sqrt{2\pi\sigma_j^2}}\exp\left[-\frac{(x_j-x'_je^{-1/2\gamma_j\tau})^2}{2\sigma_j^2}\right],$$
$$\sigma_j^2=\frac{1}{4\gamma_j}(1-e^{-\gamma_j\tau}). \quad (23)$$

Remarkably, the diffusion coefficients σ_j^2 remains positive for all times, both below ($2\kappa<\Gamma$) and above ($2\kappa>\Gamma$) threshold. However, from the physical point of view, Eq. (20) provides a good description of the amplifier above threshold only for short times, namely when saturation effects can be neglected. Of course, Eq. (20) admits a stationary solution only below threshold: such a solution can be easily derived from Eqs. (21) and (22) and, independently on the initial state, it has the Gaussian form

$$W'_{\rm stat}(x_1,y_1;x_2,y_2)=\frac{16\gamma_+\gamma_-}{\pi}\exp[-4\gamma_+(x_1^2+y_2^2)$$
$$-4\gamma_-(x_2^2+y_1^2)], \quad (24)$$

corresponding to the (factorized) squeezed thermal density matrix given by

$$\hat{\varrho}'_{stat}=[S_c(r)\hat{\nu}_{c\bar{N}}S_c^\dagger(r)]\otimes[S_b(-r)\hat{\nu}_{b\bar{N}}S_b^\dagger(-r)]. \quad (25)$$

In Eq. (25) $\hat{S}_a(r)=\exp[(r/2)(a^{\dagger 2}-a^2)]$ denotes the squeezing operator for mode a, whereas $\hat{\nu}_{a\bar{N}}$ is the density matrix of a thermal state with $\bar{N}$ thermal photons

$$\hat{\nu}_{a\bar{N}}=\frac{1}{1+\bar{N}}\left(\frac{\bar{N}}{1+\bar{N}}\right)^{a^\dagger a}. \tag{26}$$

Both the squeezing parameter r and the thermal photon number $\bar{N}$ in Eq. (25) only depend on the ratio between 2κ and Γ, in formula

$$r=\frac{1}{4}\ln\frac{\gamma_+}{\gamma_-}, \qquad 2\bar{N}+1=\frac{1}{2}\frac{1}{\sqrt{\gamma_+\gamma_-}}. \tag{27}$$

The stationary solution $\hat{\varrho}_{stat}$ for the original Master equation (14) can be obtained through Eq. (16), and it is given by

$$\hat{\varrho}_{stat}=\exp[2r(c^\dagger b^\dagger-cb)][\hat{\nu}_{c\bar{N}}\otimes\hat{\nu}_{b\bar{N}}] \times\exp[-2r(c^\dagger b^\dagger-cb)]. \tag{28}$$

Let us now consider the more interesting case of amplification above threshold. The Wigner function $W_\tau(x_1,y_1;x_2,y_2)$ corresponding to the evolved density matrix $\hat{\varrho}_\tau$ can be obtained from $W'_\tau(x_1,y_1;x_2,y_2)$ by noticing that the unitary transformation $\hat{V}$ in Eq. (15) just corresponds, at all times, to a rotation in the four-dimensional space for the Wigner function. More explicitly

$$W_\tau(x_1,y_1;x_2,y_2)=W'_\tau\left(\frac{x_1+x_2}{\sqrt{2}},\frac{y_1+y_2}{\sqrt{2}};\frac{x_2-x_1}{\sqrt{2}},\frac{y_2-y_1}{\sqrt{2}}\right). \tag{29}$$

The recipe to solve the dynamics of the amplifier is thus the following: starting from the Wigner function of the initial state $W_0(x_1,y_1;x_2,y_2)$ one evaluates $W'_0(x_1,y_1;x_2,y_2)$ by the inverse rotation of that of Eq. (29), namely,

$$W'_0(x_1,y_1;x_2,y_2)=W_0\left(\frac{x_1-x_2}{\sqrt{2}},\frac{y_1-y_2}{\sqrt{2}};\frac{x_2+x_1}{\sqrt{2}},\frac{y_2+y_1}{\sqrt{2}}\right). \tag{30}$$

Then, one makes $W'_0(x_1,y_1;x_2,y_2)$ evolve according to Eq. (22), and finally recovers $W_\tau(x_1,y_1;x_2,y_2)$ by means of Eq. (29). Following this recipe we have numerically simulated the whole evolution, starting from the Wigner function of the state (3), namely,

$$W_0(x_1,y_1;x_2,y_2)=\frac{8}{\pi^2}\exp[-2(x_1^2+x_2^2+y_1^2+y_2^2)] \times[(x_1\cos\delta+y_1\sin\delta-x_2)^2 +(y_1\cos\delta-x_1\sin\delta-y_2)^2-\tfrac{1}{2}]. \tag{31}$$

The input state is nonclassical and exhibits negative values in the Wigner function. The Green evolution can be performed by standard Monte Carlo techniques, by evolving separately the positive and negative parts of the Wigner function, which are not mixed by the Fokker-Planck equation (20). In Fig. 3

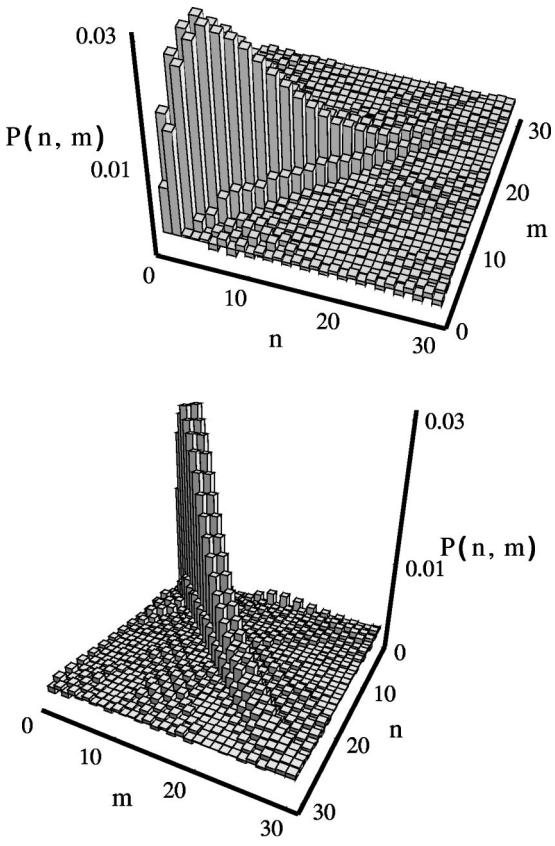

FIG. 3. The two-mode photon distribution $P(n,m)$ for $\delta=0$ and for $2\kappa/\Gamma=30$. The corresponding interaction time is given by $\tau=0.1$. We report two views of the distribution. In comparison with the ideal case of Fig. 2 the main effect of losses is the appearance of subdiagonal terms, however, without affecting the high correlation between the modes.

we report the two-mode number probability $P(n,m)$ which, in terms of the Wigner function, reads

$$P(n,m)=\frac{4}{\pi^2}(-1)^{n+m}\int_{\mathbb{R}}\int_{\mathbb{R}}\int_{\mathbb{R}}\int_{\mathbb{R}}dx_1dy_1dx_2dy_2 \times W(x_1,y_1;x_2,y_2)e^{-2(x_1^2+y_1^2+x_2^2+y_2^2)} \times L_n[4(x_1^2+y_1^2)]L_m[4(x_1^2+y_1^2)], \tag{32}$$

$L_n[x]$ being the nth Laguerre polynomial. The plot is obtained for a threshold ratio $2\kappa/\Gamma=30$, and for $\delta=0$. The effectiveness of the amplification process above threshold is apparent. We have chosen a short interaction time in order to have saturation effects negligible. Notice that the main effect of losses is the appearance of additional subdiagonal terms, however, as compared to Fig. 2, without affecting the high correlation between the two modes. On the other hand, the amplification below threshold cannot stem the detrimental effect of losses, and the field state rapidly approaches the thermal-squeezed state of Eq. (25). By varying the optical paths of the input beams, namely the value of δ, we have also evaluated the correlation function $\mathsf{C}^{(2)}$ defined in Eq. (11). In Fig. 4 we report $\mathsf{C}^{(2)}$ for different values of the

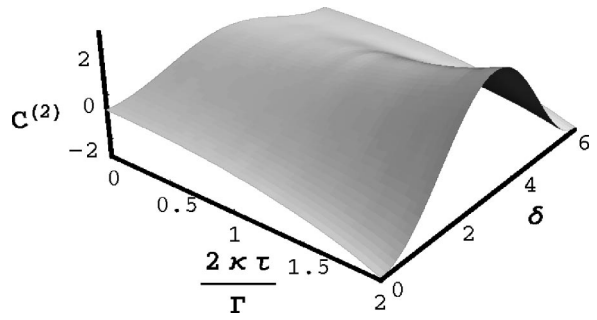

FIG. 4. The correlation function $C^{(2)}$ as a function of the ratio $2\kappa\tau/\Gamma$ and the phase shift δ. Compare Eq. (12) for the lossless case.

effective gain $2\kappa\Gamma/\tau$. By inspecting the dependence of $C^{(2)}$ on the phase shift δ in Fig. 4 one immediately argues that in a wide range of working regimes the effects of losses does not wash out the interference fringe.

IV. CONCLUSIONS

In this paper we analyzed the effect of losses on the visibility of mesoscopically entangled superpositions generated by stimulated down-conversion according to the schemes proposed in Ref. [11]. The setup relies on feeding a nondegenerate parametric amplifier by a quantum seed, which is a single-photon state with indistinguishable signal and idler paths. At the output of the amplifier we have an entangled state, with the entanglement shared by a couple of spatially separated field modes. In the experiment currently running in the Quantum Optics Laboratory of the University of Roma (adopting a 0.5 W Ti: sapphire MIRA coherent laser) the value of the gain ranges from 0.01 to 0.1 depending on the state of focalization of the uv pump beam. After the adoption (in the near future) of an additional regenerative parametric amplifier, the value of the gain will be further multiplied by a factor of about 20. We analyzed the full amplification process taking into account the effects of losses. We have shown that the preparation of mesoscopic entanglement works effectively with the amplifier above threshold, for short interaction times. The resulting superposition is robust against decoherence and can be revealed by a simple interference measurement.

ACKNOWLEDGMENTS

This work has been cosponsored by MURST under the project ''Amplificazione e rivelazione di radiazione quantistica.'' M.F.S. is supported by INFM through Project No. PRA-CAT-1997.

[1] C.H. Bennett, Phys. Scr. **T76**, 210 (1998).
[2] *Introduction to Quantum Computation and Information*, edited by H-K. Lo, S. Popescu, and T. Spiller (World Scientific, Singapore, 1998).
[3] D. Bouwmeester, J.W. Pan, K. Mattle, M. Eibl, H. Weinfurter, and A. Zeilinger, Nature (London) **390**, 575 (1997); D. Boschi, S. Branca, F. De Martini, L. Hardy, and S. Popescu, Phys. Rev. Lett. **80**, 1121 (1998); S.L. Braunstein and H.J. Kimble, *ibid.* **80**, 869 (1998).
[4] See, for example, J. Mod. Opt. **44**, No. 11-12 (1997), special issue on quantum state preparation and measurement, edited by M. G. Raymer and W. P. Schleich.
[5] G. M. D'Ariano, in *Latest Developments in Quantum Tomography*, edited by P. Kumar *et al.*, in Quantum Communication, Computing and Measurement (Plenum, New York, 1999).
[6] D. N. Klyshko, *Photons and Nonlinear Optics* (Gordon and Breach, New York, 1988).
[7] Z.Y. Ou, L. Mandel, Phys. Rev. Lett. **61**, 50 (1988); J.G. Rarity and P.R. Tapster, *ibid.* **64**, 2495 (1990); M.H. Rubin and Y.H. Shih, Phys. Rev. A **45**, 8138 (1992); P.G. Kwiat, K. Mattle, H. Weinfurther, and A. Zeilinger, Phys. Rev. Lett. **75**, 4337 (1995).
[8] W. Tittel, G. Ribordy, and N. Gisin, Phys. World **11**, 41 (1998).
[9] F. De Martini, Phys. Rev. Lett. **81**, 2842 (1998).
[10] F. De Martini, M. Fortunato, P. Tombesi, and D. Vitali, Phys. Rev. A **60**, 1636 (1999).
[11] F. De Martini, Phys. Lett. A **250**, 15 (1998).
[12] F.A. Bovino, F. De Martini, and V. Mussi, e-print quant-ph/9905048.
[13] G.M. D'Ariano and M.F. Sacchi, Mod. Phys. Lett. B **11**, 1263 (1997).